New Folder Name 40m Prototype

Characterization of the Caltech 40 meter prototype seismic isolation stack

Measurements and models

N. Mavalvala, L. Sievers, D. Shoemaker

MIT-Caltech LIGO Science team

September 10, 1991

1 Abstract

A series of transfer function measurements were made on the Caltech 40 meter prototype stack to get a more complete understanding of the behavior of the stack, to compare it with two-dimensional models, and to predict accurately the contribution of the ground noise spectrum to the 40 meter prototype strain spectrum. Transfer functions were measured for the two elastomers in use in the 40 meter prototype, rubber cars and silicone cubes, along two axis: (a) vertical (z) axis excitation, and (b) horizontal (x or optic) axis excitation. Good agreement with the two-dimensional model is found for low frequencies; at higher frequencies, deviations from the model are due to internal resonances in the physical stack masses. Isolation no better than 10^{-5} is achieved by a three-stage stack.

2 Introduction

Our goal is to determine the net motion along the optic axis of the suspended mirror test mass in the 40 meter prototype. To do this, we must characterize the seismic excitation, the isolation stack transfer function, and the test mass pendular suspension. Here we will address the question of the stack transfer function.

The isolation system is shown schematically in Figure 1. If the support structure for the stack (the stack suspension points) and the top plate are assumed to be perfectly rigid, a complete characterization of the linear stack properties is made with measurements of the transfer function matrix for the six degrees of freedom of excitation (x, y and z translational axes and θ_x, θ_y and θ_z rotational axes) to the six degrees of freedom of the motion of the top of the stack. In general we would need all six degrees of freedom, but if we align the principal axes of the springs with the symmetry axes of the system, we reduce the system to a rigid body confined to a plane. Then several elements of the transfer function matrix are unimportant for the motion of the test mass mirror along the optic axis. The three coordinates for the remaining degrees of freedom are x,z and θ, as shown in Figure 2. Clearly the transfer function matrix element, x/x_g, of horizontal excitation (along the optic axis; x_g is the ground motion along the optic axis) to horizontal motion of the pendulum suspension is important. From the model we find that vertical excitations couple to the rotational motion of the top plate. This is consistent with the expectation that the asymmetry of the 'horseshoes' (lead masses) will cause the motion in a given direction to cross-couple to other

directions due to rotation of the masses. The predictions of the model coupled with empirical observations motivate the following transfer function elements to be measured for both elastomers (see Figure 2 for axis labels):

(i) x_{cm}/x_g

(ii) x_{cm}/z_g

(iii) x_{edge}/z_g

(iv) z_{cm}/z_g

(v) y_{cm}/z_g

(vi) z_{cm}/x_g

(vii) y_{cm}/x_g

Measurements (i) and (ii) are made for the above reasons. From measurement (iii) we can get the tilt coefficient due to rotational motion. Measurement (iv) is important because vertical motion can couple to the x-motion of the pendulum. Measurements (v), (vi) and (vii) are made for completeness, to ensure that we understand the cross-coupling in all three directions. In addition to these measurements, we measured power spectra for in-plane and out-of-plane horseshoe modes as well, in order to identify internal resonances that contaminate the stack transfer functions. Finally, we also performed compression and shear measurements on a single stage stack to extract the elastomer properties of the cars and cubes using a four pole parameter model, which we describe in the section 4. It should be noted that we did not attempt to measure or characterize the possible non-linearities or upconversion mechanisms that might exist in this stack design.

Before we proceed to describe the measurements, we should elaborate on the 40 meter prototype isolation system. The support structure consists of four posts to which the supports for the bottom plate are attached, as shown in Figure 1. As mentioned earlier, we assume that the support structure is perfectly rigid and does not contribute to the transfer functions[1]. The stack itself has three stages, the bottom two stages consisting of a lead horseshoe-shaped mass (three sides of a square) sitting on four springs, one at each corner of the horseshoes. The top stage uses the pendulum suspension structure (the so-called 'top plate') as the mass (m_3 in Figure 2). The test mass is suspended as a pendulum from the top plate; in the current 40 meter prototype system, there is an additional intermediate mass (called the 'control block') which allows a marionette-like control over the two

[1] This is not the case; Mike Burka demonstrated, using finite element modelling, that the four-post structure probably has several excitable resonances in the frequency range of interest.

angles of the test mass. This pendulum suspension give some additional filtering, although its complexity may result in some differences from the $1/f^2$ behavior expected for a simple pendulum.

The 40 meter prototype stacks use elastomers as springs, since they have good damping properties. While the cars have a lower Q (mechanical quality factor), and therefore better damping, their vacuum properties are highly unsatisfactory. They outgas oily hydrocarbons that may be responsible for corrupting the vacuum system. They have been partially replaced by cubes made of silicone RTV, which are significantly better behaved in vacuum than their predecessors, but have a considerably higher Q. In principle, each stage of the stack should contribute $1/f^2$ isolation, i.e. $1/f^6$ for the three-stage stack. At higher frequencies, however, the transfer function deviates from this $1/f^6$ isolation due to internal modes of the masses.

3 Experimental method

Figure 3 (a) and 3 (b) describe the arrangements for measurements with horizontal (x) and vertical (z) excitation, respectively. For horizontal excitation, we suspend the bottom plate by three 1 meter long tungsten wires. The length of the wire is chosen to ensure that the violin modes of the wire under tension do not lie in the low frequency region of the transfer function. We do not see the violin modes couple into the transfer functions. The bottom piece is a 12"x 12"x 1" aluminum plate with mounts for the accelerometers and a means to attach the plate rigidly to an electromagnetic shaker. The horseshoes are 11"x 11" and are stacked on top of each other, separated by a layer of four rubber cubes (cars). The centers of the cubes are nominally 3/4" from each of the horseshoe edges. It is worth noting that the transfer functions are not greatly altered when the position of the cubes is changed, but small differences are present. The main features of the transfer function are not affected by the exact physical configuration of the stack. We have measured transfer functions with two kinds of top plates: the one is an 11"x 11"x 1" aluminium plate and the second is an odd-shaped aluminium plate that rests on ball bearing pivots on two 11"x 11"x 1/4" steel horseshoes, which are themselves separated by two ball bearings. For either top plate, we take the center of mass to be at the geometric center, which is correct, given the symmetry of

the structures. Endevco (7707–1000) accelerometers are placed at the geometric center of the bottom plate and at the center of mass or the edge of the top plate, depending on whether a direct coupling or tilt coupling is being measured. The signal from the accelerometers is amplified by low noise amplifiers. Since the accelerometer on the bottom plate has more signal at almost all frequencies, we used a home-made OP27 amplifier circuit with 20 dB gain. The output of the accelerometer on the top plate is amplified using a Stanford SR650 with a low pass filter at 2.6 kHz and 40 dB gain. The amplified signals are then fed into an HP spectrum analyzer and the transfer function and coherence are measured. The signals are never limited by electronic noise in the measurement frequency range (1 Hz to 1 kHz).

For vertical excitation, a similar apparatus is used. We modify the tungsten wires by adding coil springs to which the bottom plate is attached. This scheme is necessary to allow enough freedom in the vertical direction, without putting the entire load on the shaker armature. The shaker is attached to the bottom plate at the crudely measured center of mass of the bottom plate and stack[2]. For transfer functions in this configuration we find a large resonance at about 600 Hz. This turns out to be an internal "drumhead" resonance of the bottom plate, and we can reduce this feature by placing the bottom accelerometer at the edge of the plate. The signal amplification and transfer function measurements are made in the same way as for horizontal excitation.

In presenting the experimental data, we find that precious little stands to be gained by showing all of the measured transfer functions. Far more central to the investigation at hand is the correlation between the various transfer functions as predicted by the model and their corresponding experimental counterparts. These are shown in Figure 8 and a detailed analysis is presented in the Section 4.

One of the most persistent problems we have been faced with is acoustic pick-up either by the accelerometers or by the top plate acting as a microphone. For frequencies greater than 60 Hz the transfer function simply levels off to a constant -75 dB plateau due to acoustic pick-up. Conventional shielding methods such as lead impregnated foam or headphone cups are unable to lower the pick-up by more than a few dB. To resolve this we performed a set of measurements in vacuum for vertical excitation (for which the acoustic pick-up was more problematic since the bottom and top plate formed a resonating cavity between them). The experimental

[2] The center of mass of the bottom plate loaded with the stack is determined by balancing them on a cylindrical rod.

set up is illustrated in Figure 4. The scheme with the steel ring and the aluminium "Y" piece is just incidental since it was already set up for experiments on the LIGO prototype stacks. The tests in vacuum proved to be very useful; we are no longer limited by acoustic feed through and are able to measure a stack attenuation of -120 dB, which is low enough for us to adequately measure the transfer function at higher frequencies. A comparison of the in-air and in-vacuum measurements are shown in Figure 5.

We have also measured transfer functions for a single stage stack for both horizontal and vertical excitation, with the primary purpose of extracting the compression and shear moduli of the elastomers. This is done using a four pole parameter model, which incorporates a spring and dashpot in series and both in parallel with another spring as shown in Figure 7 (e); the fits of this model to the data are shown in Figure 7 (a) through (d). This model is not ideally suited to the problem at hand, but parameters derived using this model fit the experimental data well, as we show in the next section.

Finally, Figure 6 (a) and (b) show power spectra for in-plane and out-of-plane excitation of the horseshoes, respectively, when they are freely suspended. These measurements were made by suspending the horseshoe and tapping it in the y-direction and the z-direction, respectively, with an accelerometer placed on the horseshoe to detect the desired motion.

4 Stack modelling

Figure 2 shows a 2 dimensional schematic diagram of a 3 stage spring mass isolation stack. The three masses are modeled as rigid bodies. Each of the mass elements is connected to the next mass element at two locations by pieces of rubber or silicone cubes. The rubber and silicone cubes are initially modeled as simple springs. The two lower masses represent the horseshoes in the 40 meter prototype stack and the top mass represents the top plate. Each mass is allowed three degrees of freedom; rotation, vertical translation, and horizontal translation. The laser beam axis is defined as the x axis.

The model used in this analysis is more complicated than the model in the 1989 proposal since more of the stack's dynamical features are included. In this

model the center of mass of each element is not necessarily at the geometric center of the element. This feature is added to account for the uneven mass distribution of the horseshoes and the uneven mass-loading of the top plate. Equations of motion for the 2–dimensional stack model are as follows:

$$
\begin{aligned}
m_1\ddot{z}_1 &= k_z[-4z_1 + 2z_2 + 2z_g + 2(r_{11} - r_{12})\Theta_1 - (r_{21} - r_{22})\Theta_2] \\
m_2\ddot{z}_2 &= k_z[-4z_2 + 2z_3 + 2z_1 - (r_{11} - r_{12})\Theta_1 + 2(r_{21} - r_{22})\Theta_2 - (r_{31} - r_{32})\Theta_3] \\
m_3\ddot{z}_3 &= k_z[-2z_3 + 2z_2 - (r_{21} - r_{22})\Theta_2 + (r_{31} - r_{32})\Theta_3] \\
m_1\ddot{x}_1 &= k_x[-4x_1 + 2x_2 + 2x_g - 2(p_{11} - p_{12})\Theta_1 + 2p_{21}\Theta_2] \\
m_2\ddot{x}_1 &= k_x[-4x_2 + 2x_3 + 2x_1 - 2p_{12}\Theta_1 - 2(p_{21} - p_{22})\Theta_2 + 2p_{31}\Theta_3] \\
m_3\ddot{x}_3 &= k_x[-2x_3 + 2x_2 - 2p_{22}\Theta_2 - 2p_{32}\Theta_3]
\end{aligned}
$$

$$
\begin{aligned}
I_1\ddot{\Theta}_1 = {} & k_x[(p_{11} + p_{12})x_g - (p_{11} + p_{12} - p_{22} - p_{21})x_1 - (p_{21} + p_{22})x_2 \\
& - (p_{12}^2 + p_{11}p_{12} + p_{12}p_{22} + p_{12}p_{21})\Theta_1 - (p_{22}^2 + p_{21}p_{22})\Theta_2] \\
& + k_z[(-r_{11} + r_{12})z_g + (r_{11} - r_{12} + r_{21} - r_{22})z_1 - (r_{21} - r_{22})z_2 \\
& - (r_{11}^2 + r_{12}^2 + r_{11}r_{21} + r_{12}r_{22})\Theta_1 + (r_{21}^2 + r_{22}^2)\Theta_2]
\end{aligned}
$$

$$
\begin{aligned}
I_2\ddot{\Theta}_2 = {} & k_x[(p_{21} + p_{22})x_1 - (p_{21} + p_{22} - p_{31} - p_{32})x_2 - (p_{31} + p_{32})x_3 - (p_{12}p_{22} + p_{12}p_{21})\Theta_1 \\
& - (p_{22}^2 + p_{21}p_{22} + p_{22}p_{32} + p_{22}p_{31})\Theta_2 - (p_{32}^2 + p_{31}p_{32})\Theta_3] \\
& + k_z[(r_{22} - r_{21})z_1 + (r_{21} - r_{22} + r_{31} - r_{32})z_2 + (r_{32} - r_{31})z_3 + (r_{12}r_{22} + r_{11}r_{21})\Theta_1 \\
& - (r_{22}^2 + r_{21}^2 + r_{22}r_{32} + r_{21}r_{31})\Theta_2 + (r_{32}^2 + r_{31}^2)\Theta_3]
\end{aligned}
$$

$$
\begin{aligned}
I_3\ddot{\Theta}_3 = {} & k_x[(p_{31} + p_{32})x_2 - (p_{31} + p_{32})x_3 - (p_{22}p_{32} + p_{22}p_{31})\Theta_2 - (p_{32}^2 + p_{31}p_{32})\Theta_3] \\
& + k_z[(r_{32} - r_{31})z_2 - (r_{32} - r_{31})z_3 + (r_{22}r_{32} + r_{21}r_{31})\Theta_2 - (r_{31}^2 + r_{32}^2)\Theta_3]
\end{aligned}
$$

where the symbols have the following meanings:

1. m_i = i'th mass
2. z_i = vertical translation of center of mass of m_i
3. x_i = horizontal translation of center of mass of m_i
4. Θ_i = rotation of m_i about its center of mass

5. r_{ij} = horizontal distance of spring from horizontal center of mass of m_i.
($j = 1$ is left spring, $j = 2$ is right spring)
6. p_{ij} = vertical distance of spring from vertical center of mass of m_i.
7. ($j = 1$ is bottom spring, $j = 2$ is top spring)
8. x_g = horizontal ground motion
9. z_g = vertical ground motion
10. k_x = horizontal spring stiffness
11. k_z = vertical spring stiffness
12. k_{1x}, k_{2x}, c_x = 3 spring parameter model in horizontal direction
13. k_{1z}, k_{2z}, c_z = 3 spring parameter model in vertical direction

The equations above were derived assuming that the silicone cubes or the rubber cars behave as simple spring elements with constant horizontal and vertical stiffness parameters k_x and k_z. The dynamical properties of the cubes and the cars can be more accurately modeled using a spring and a dashpot in series, and the series combination in parallel with another spring. This model is termed the 4 pole spring model (see Figure 7 (e)) and is commonly used for modeling the dynamical properties of an elastomer. Both the rubber cars and the silicone cubes were fit to this model. The fits of the measured data were not always robust, but the numerical predictions for the stack transfer functions using the fitted parameters (i.e., $k_{1x}, k_{2x}, c_x, k_{1z}, k_{2z} c_z$) compared well with the measurements taken for the stack transfer function. (For the case of the rubber cars in the $z$direction, a 'fit by hand' was performed because poor data made a computer fit unreliable.) Figure 7 (a) through (d) shows the fit between the model and experiment for both cars and cubes in compression and shear.

It is a two-step process to change the equations of motion derived earlier so that the model of the stack includes the effects of the elastomers modeled with the 4 pole spring model. The first step is to write the 9 equations of motion in terms of their Laplace transforms. The second step is to replace the constant spring stiffness functions k_x and k_z with the frequency dependent spring stiffness functions $k_x(s)$ and $k_z(s)$, respectively. The functions $k_x(s)$ and $k_z(s)$ are defined by their corresponding 4 pole model parameters and the Laplace variable s:

$$k_x(s) = k_{1x} + \frac{k_{2x}c_x s}{k_{2x} + c_x s}$$

$$k_z(s) = k_{1z} + \frac{k_{2z}c_z s}{k_{2z} + c_z s}$$

Transfer functions from the ground motion to the top plate motion can be derived from the resulting ensemble of equations. This is the version of the model that most accurately predicts the dynamics of the 40 m isolation stack. The relevant transfer functions for vibration isolation have been plotted using this model against their experimental counterparts for comparison and analysis. These plots are discussed in Section 5

5 Measured and calculated transfer functions

Figures 8.1-8.6 are the transfer functions for a stack with a simple top plate and silicone cubes for springs. Figures 8.1 and 8.2 show the transfer functions from horizontal ground motion to horizontal motion at the center of mass of the top plate and from vertical ground motion to vertical motion at the center of mass of the top plate, respectively. Above roughly 120 Hz the experimental transfer function is dominated by acoustic pickup. The experimental and modeled horizontal to horizontal transfer functions show a high degree of correlation at frequencies below 30 Hz but the experimental data deviates significantly above 30 Hz. It is believed that the horseshoe resonances start dominating the spectrum in this range (the resonances were not modeled). When plot 1 is overlapped with the power spectra of the lead horseshoes, the peaks of the horseshoe resonances overlap the peaks in the transfer function above 30 Hz. The correlation between the vertical to vertical transfer functions is good over all frequencies below 100 Hz.

Most of the measurements that were taken are difficult to interpret above 100 Hz because they were taken in air and the acoustic coupling between the driving plate (stack support) and the stack top plate contributed to the transfer function. Figure 8.3 (an extension of 8.1 to 1 kHz) shows a broad plateau above roughly 150 Hz which is due to this coupling; some of the undulations in the plateau may be real features. The exception to this rule is the vertical to vertical transfer functions taken in vacuum. Figure 8.4 (an extension of 8.2, taken in vacuum)

shows features due to the horseshoe resonances around 270, 300, 420 and 430 Hz; see Figure 6 for reference.

Figures 8.5 and 8.6 are not as straightforward to interpret. They show the transfer functions from horizontal ground motion to vertical top plate motion and vertical ground motion to horizontal top plate motion, respectively. At low frequencies (i.e. frequencies between 1 and 4 Hz) it is believed that the experimental data shows less attenuation than the model data because the vertical drive has some unavoidable horizontal component. The explanation for the difference in the transfer functions above 30 Hz is the same as for the horizontal to horizontal transfer function and the vertical to vertical transfer function: the horseshoe resonances overlap the lumped model resonances in this frequency span. The least understood part of the spectrum is between 4 and 30 Hz. The horizontal to horizontal model transfer function shows an antiresonance at 7 Hz that doesn't appear in the experimental spectrum. This may be an artifact of the measurement: The measurement could be sensitive to sensor placement, and consequently the phasing of the two sensors in the experimental spectrum may have been somewhat different than that used in the model. The vertical to vertical experimental transfer function shows somewhat better match up with the model between 4 and 20 Hz.

Figures 8.7-8.10 are the transfer functions for a stack with a simple top plate and the rubber car springs, all measured in air. The plots can be interpreted similarly to the stacks made up of silicone cubes.

The comparison of the stack model to the experimental data shows that below the first resonant frequency of the horseshoes (Figure 6), we are able to predict the actual behavior of the stack accurately in the horizontal to horizontal direction and the vertical to vertical direction. The analysis was somewhat indeterminate as to our ability to predict the behavior in the cross directions (i.e. vertical to horizontal and horizontal to vertical). It is also obvious from this study that to properly model the dynamic behavior of the stack above 30 Hz, it is necessary to include the internal modes of the horseshoes and possibly the top plate.

Two different modeling and stack design approaches have become apparent from the results of the 40 meter prototype stack analysis. The first approach is to consider using only mass elements with resonant frequencies above 400 Hz for stack design. This choice insures that a simple lumped model will accurately predict the behavior of the stack in the region of interest. The second approach is to use mass elements with resonant frequencies below 400 Hz and damp

the resonances. From a modeling perspective this approach demands a more complicated model since internal modes must be included for an accurate picture of the stack behavior. The 400 Hz frequency bound is not a hard (or possibly accurate) bound since it is chosen using a loose extrapolation on past experiences.

Our findings are summarized in Figures 9.1 and 9.2. The solid lines in Figures 9.1 and 9.2 show the result of a *calculation* of the worst expected transfer functions from an isotropic excitation at the bottom of the stack to horizontal optical axis motion (x—motion) and vertical motion at the top of the stack, respectively, using the technique of singular value decomposition. The dashed lines in Figures 9.1 and 9.2 show the *measured* worst case transfer functions. These plots are calculated by making the quadrature sum (square root of sums of squares) of the measured transfer functions.

A stack with silicone springs has been taken as the example. The plots in Figure 9.1 show that at low frequencies (<10 or 11 Hz) both measured and calculated transfer functions are dominated by the horizontal-horizontal component (x_{cm}/x_g), but for higher frequencies the transfer functions are dominated by the horizontal motion due to vertical excitation (x_{cm}/z_g). The measured and calculated plots are very similar at frequencies below 25 hertz. The difference in the measured transfer function and the calculated transfer function above 25 hertz is partially due to the internal horseshoe resonances (these modes are not included in the model) affecting the x_{cm}/z_g transfer function. Also, it is conjectured that the peaks around 31 hertz and 44 hertz in the measured transfer function are due to nonuniformities in the construction of the stack. Nonuniformities may be responsible for the added coupling between the vertical and horizontal directions. It is interesting to note that resonances at each of these frequencies appear in the vertical to vertical transfer function.

Figure 9.2 shows that the worst case transfer function in the vertical direction is dominated at all frequencies by the vertical to vertical component (z_{cm}/z_g). The measured and calculated plots show excellent agreement below 50 hertz. The internal horseshoe resonance at around 65 hertz causes an obvious deviation in the two plots at higher frequencies.

The excellent agreement in the low-frequency regime, and the simple explanation for the deviation at higher frequencies, leads us to conclude that the model of the stack given here is quite accurate given the fact that it does not include internal degrees of freedom of the masses.

6 Comparison with *in situ* stack measurement

It is important to determine the relevance of the measurements performed here to the actual implementation of the seismic isolation system as installed in the 40 meter prototype. We make here a comparison between transfer functions of the stack measured separately (i.e., with the system described in detail above) and in the 40 meter apparatus.

To measure the performance of the stack as installed, an accelerometer (B+K) was placed on the optical table supporting one of the end tanks of the 40 meter vacuum system. A second accelerometer was attached to the stack top plate. The apparatus was at atmospheric pressure for the measurement. The structure supporting the stack was included in this transfer function, as was any influence of the hanging mass. The transfer function for the horizontal-to-horizontal axis is shown in Figure 10.1, where a small shaker (B+K) was used to excite the optical table. For the vertical-to-vertical axis, the ratio of two ground-noise driven power spectra are shown in Figure 10.2

Two differences are worth noting. For the vertical-vertical transfer function, the *in situ* measurement shows a much higher transmissivity than the separate measurement for frequencies above about 75 Hz. This is probably due to changes in the ambient driving noise spectrum, and is probably not significant. The other point to note is the strong resonance around 38 Hz in the *in situ* horizontal-horizontal transfer function. This is probably due to a resonance in the support structure for the stack.

In the large scale, the overall forms are quite similar, and in general we can conclude that the stacks perform much the same way in the 40 meter apparatus and when measured separately. More detailed *in situ* measurements are needed.

7 Conclusions

The stack performance is reasonably well understood: In the frequency range from 1 to 30 Hz, very good agreement with a 2–dimensional model is found, and for higher frequencies the discrepancies can be explained by the presence of internal modes in the stack mass elements. This understanding is consistent with the present design of the LIGO prototype suspensions. In a frequency range from 10 to 100 Hz, the excitation of the 40 meter prototype pendulum suspension points is explained. To predict the low frequency 40 meter prototype strain spectrum, the pendulum suspension must be more thoroughly characterized and this work is underway.

8 Figures

1. 40 meter prototype isolation system with four post support structure and three stage stack
2. Schematic diagram of three stage isolation stack and relevant degrees of freedom
3. Experimental set-up in air for
   (a) horizontal excitation
   (b) vertical excitation
4. Experimental set-up for measurements in vacuum for vertical excitation
5. Transfer function of z_{cm}/z_g and x_{cm}/z_g in air and in vacuum
6. Power spectra of lead horseshoes for
   (a) in-plane excitation
   (b) out-of-plane excitation
7. Fit between four-pole parameter model and experiment for
   (a) cubes in compression
   (b) cubes in shear
   (c) cars in compression
   (d) cars in shear
   (e) schematic diagram of four-pole model
8. Transfer functions predicted by model and experiment for silicone cubes
   (1) x_{cm}/x_g (in air)
   (2) z_{edge}/z_g (in air)
   (3) x_{cm}/x_g to 1 kHz (in air)
   (4) z_{cm}/z_g to 1 kHz (in vacuum)
   (5) z_{cm}/x_g (in air)
   (6) x_{cm}/z_g (in air)
   Transfer functions predicted by model and experiment for rubber cars
   (7) x_{cm}/x_g (in air)
   (8) z_{cm}/z_g (in air)
   (9) z_{edge}/x_g (in air)
   (10) x_{cm}/z_g (in air)

9. Worst and best case transfer functions
   (1) calculated (in air, except for the x_{cm}/z_g contribution which was measured in vacuum)
   (2) measured (in air, except for the z_{cm}/z_g contribution which was measured in vacuum)

10. Measured and predicted top plate motion
   (1) x_{cm}/x_g
   (2) z_{cm}/z_g

Figure 1
Support structure and stack

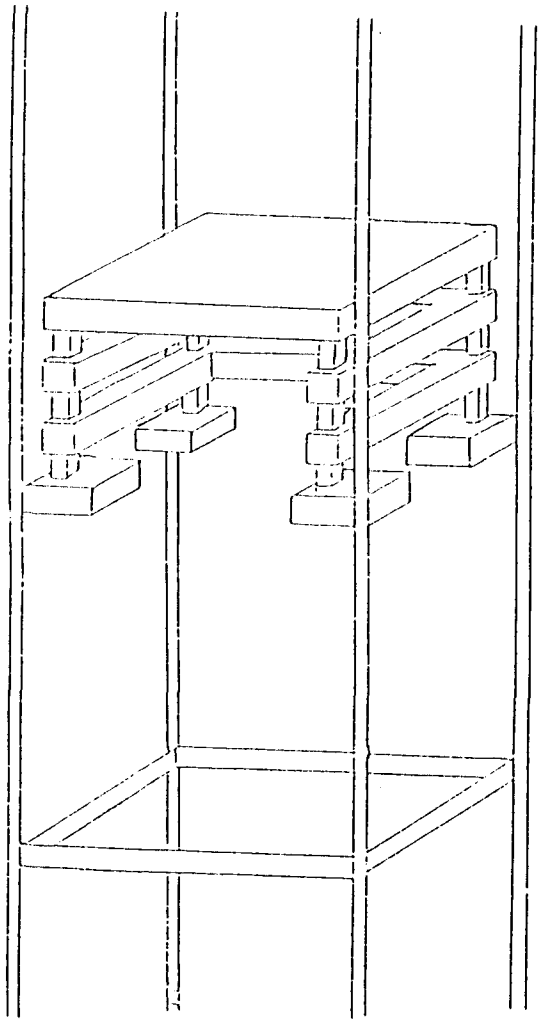

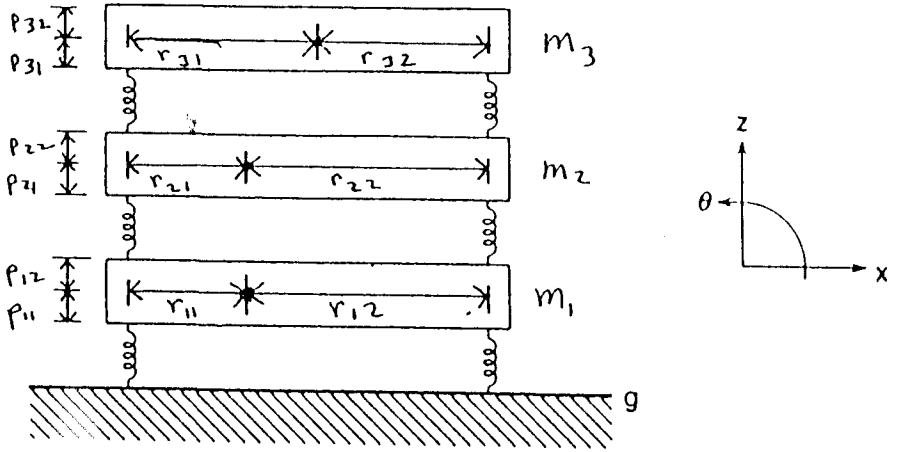

Figure 2
Schematic diagram of stack

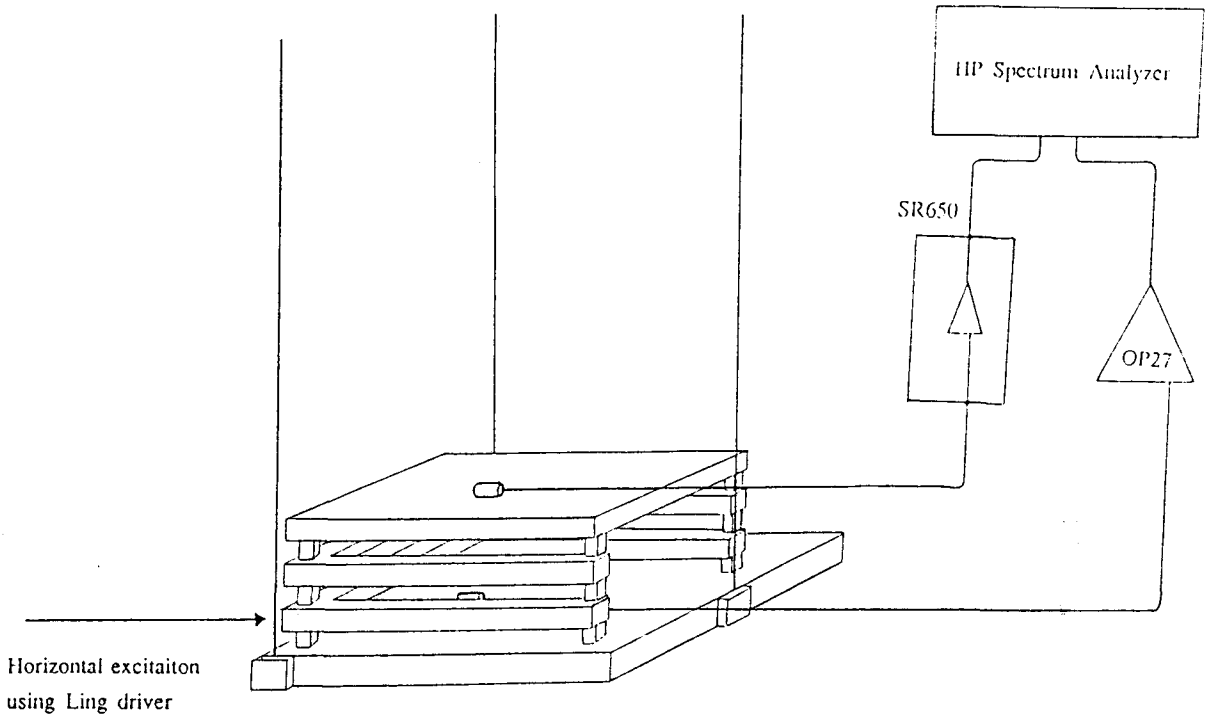

Figure 3 (a)
Horizontal excitation

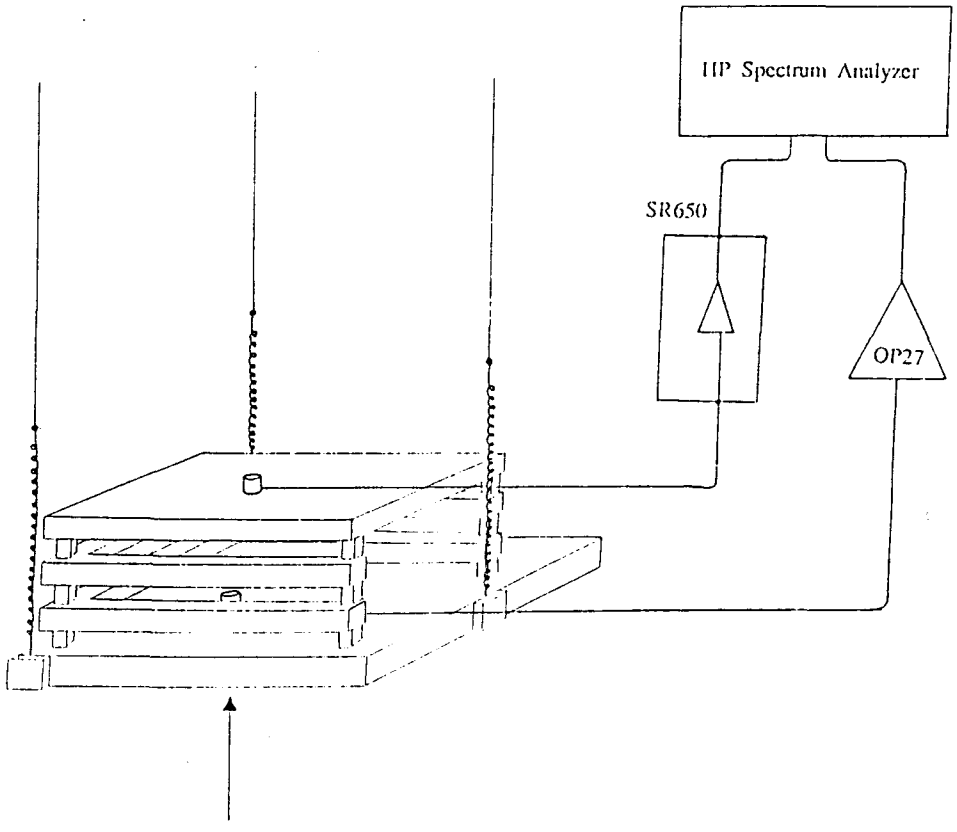

Figure 3 (b)
Vertical excitation

Figure 4
Vertical excitation in vacuum

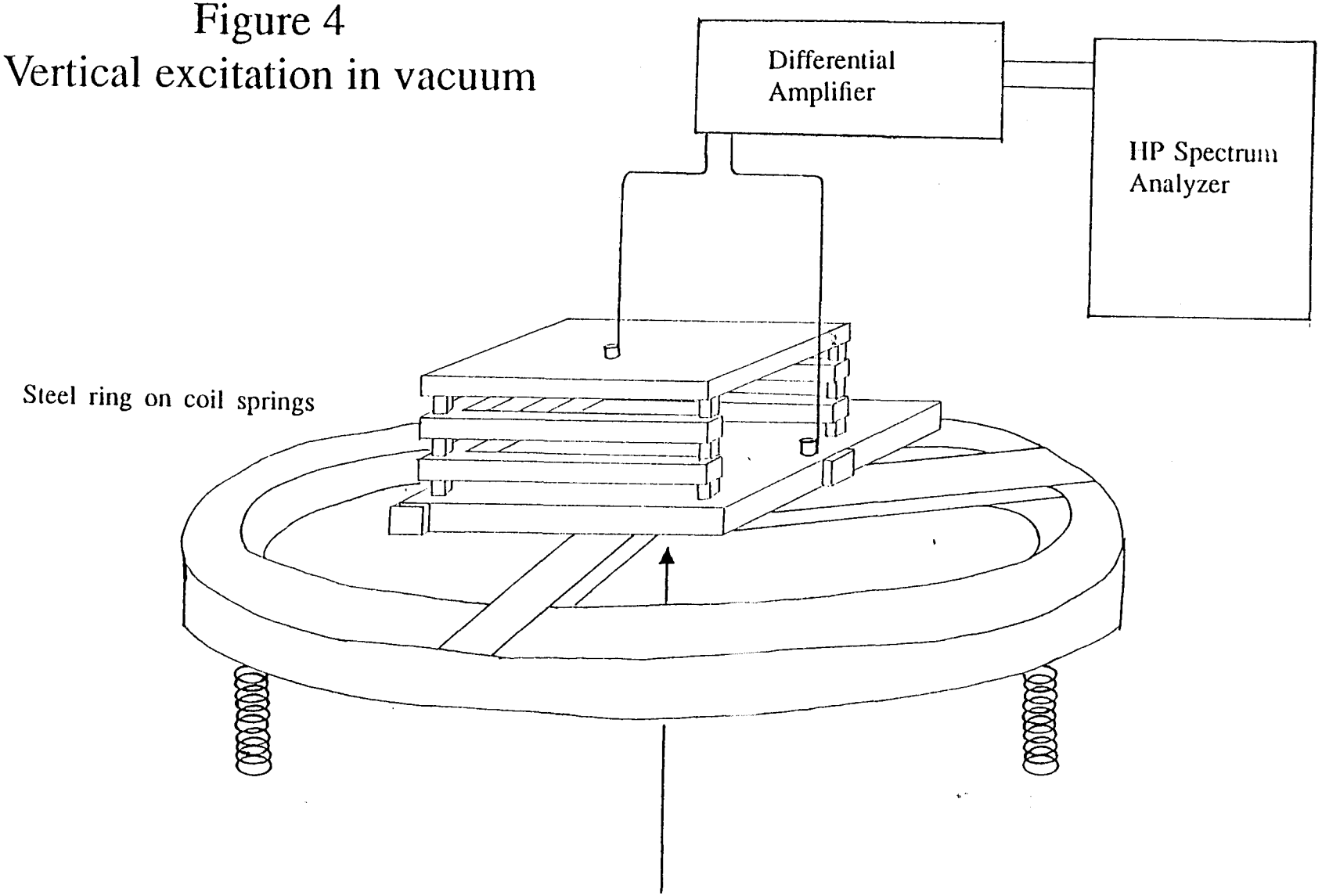

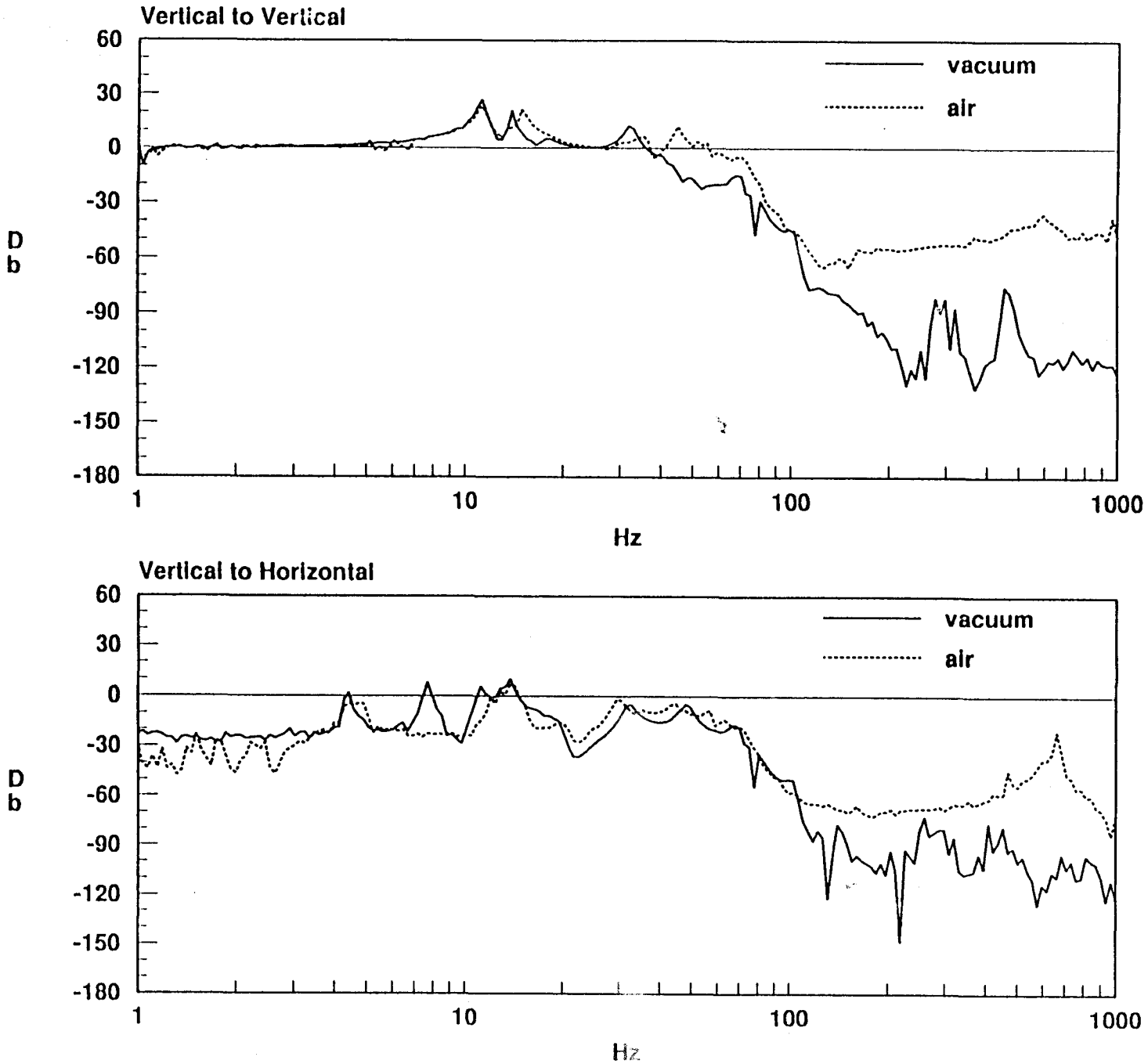

Figure 5

40M Stack TFs in air and vacuum, Silicone Springs, Simple Top Plate

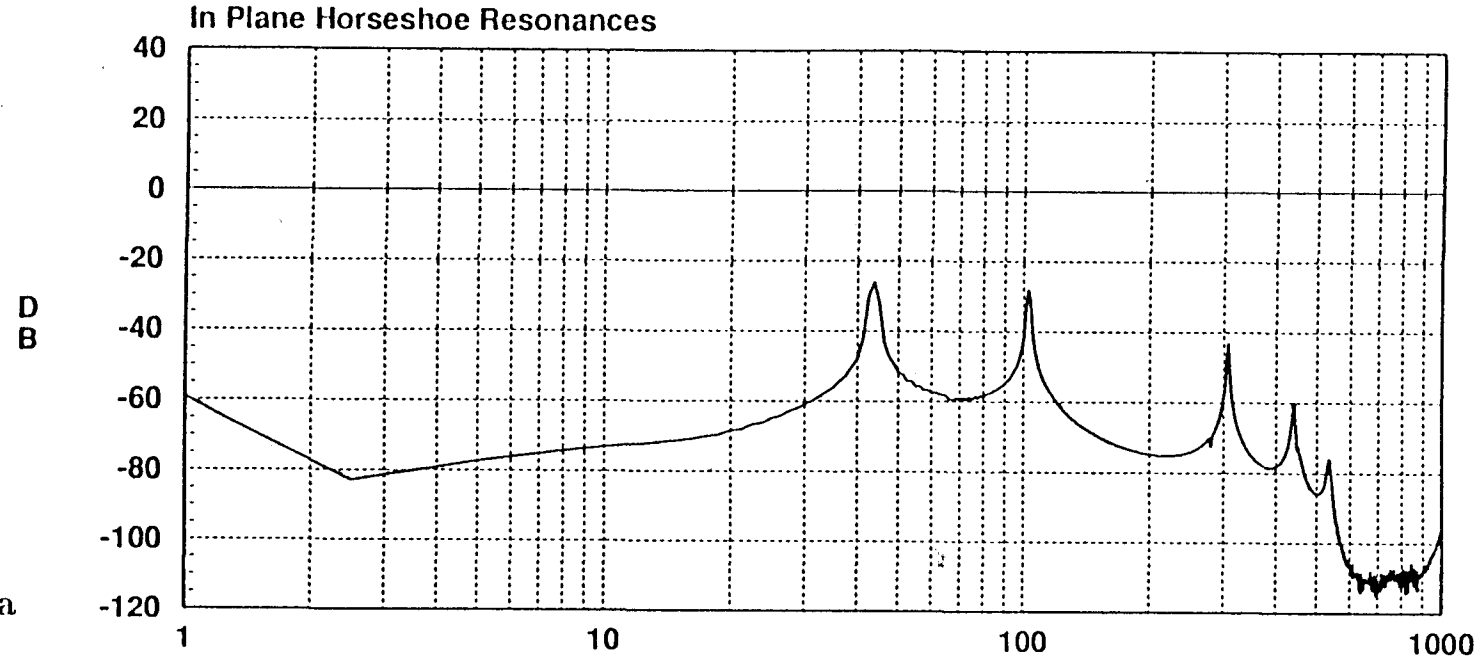

Figure 6a

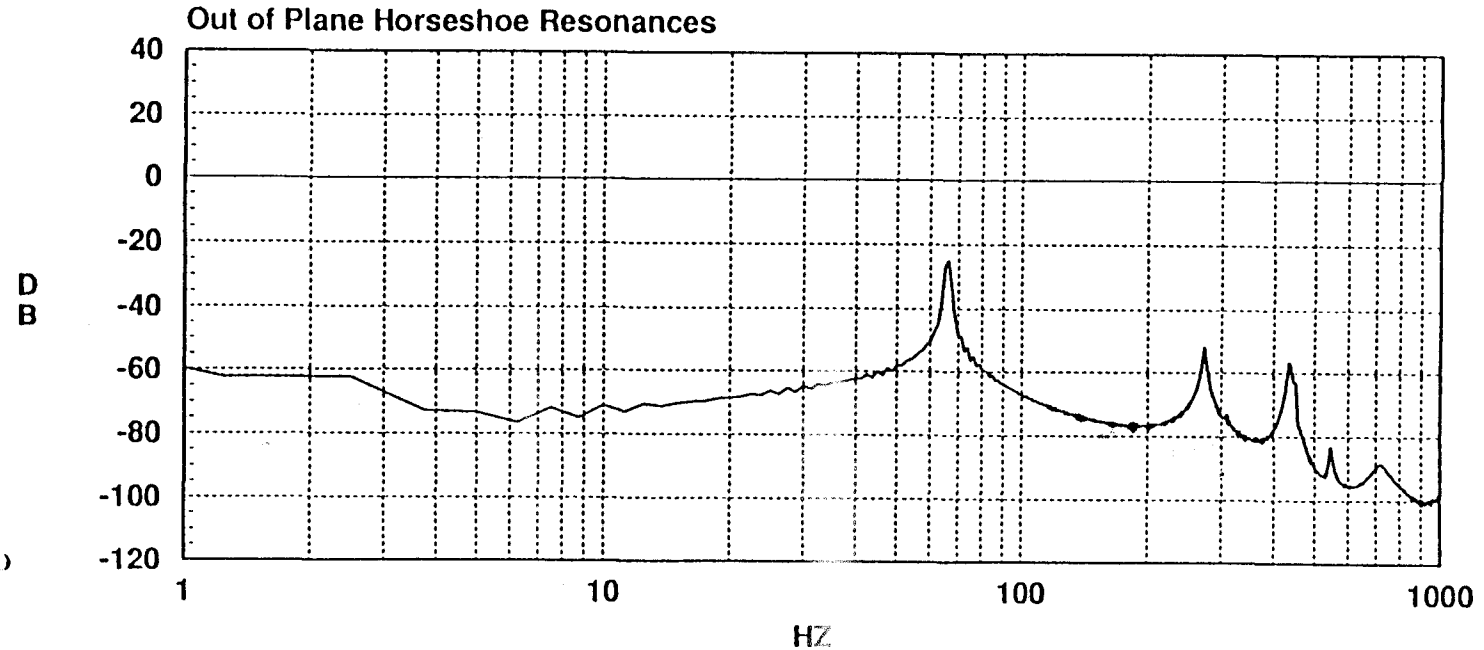

Figure 6b

Power Spectra of Lead Horseshoes used in 40 M System

Figure 7 (a)
Fit between four-pole parameter
model and experiment for
cubes in compression

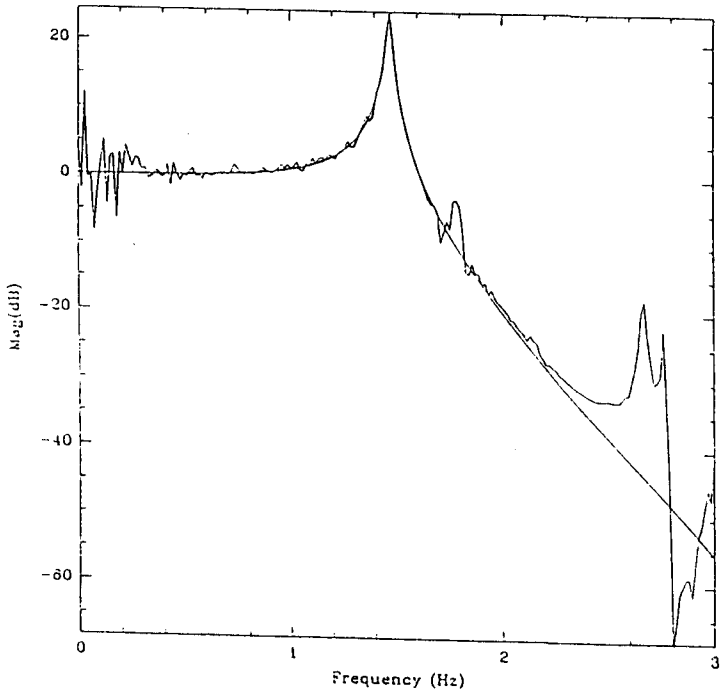

k_1=2.17e08, k_2=2.52e08, c=7.5e04
mass(kg)=6.3e0, range of fit (Hz)=5–400

Figure 7 (b)
Fit between four-pole parameter
model and experiment for
cubes in shear

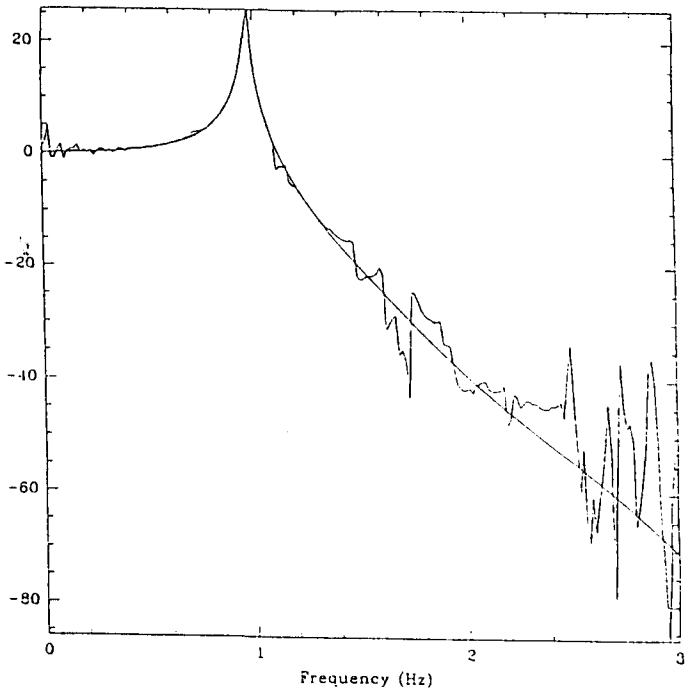

k_1=2.05e07, k_2=5.79e07, c=1.88e04
mass(kg)=5.9e0, range for fit (Hz)=5–350

Figure 7 (c)
Fit between four-pole parameter
model and experiment for
cars in compression

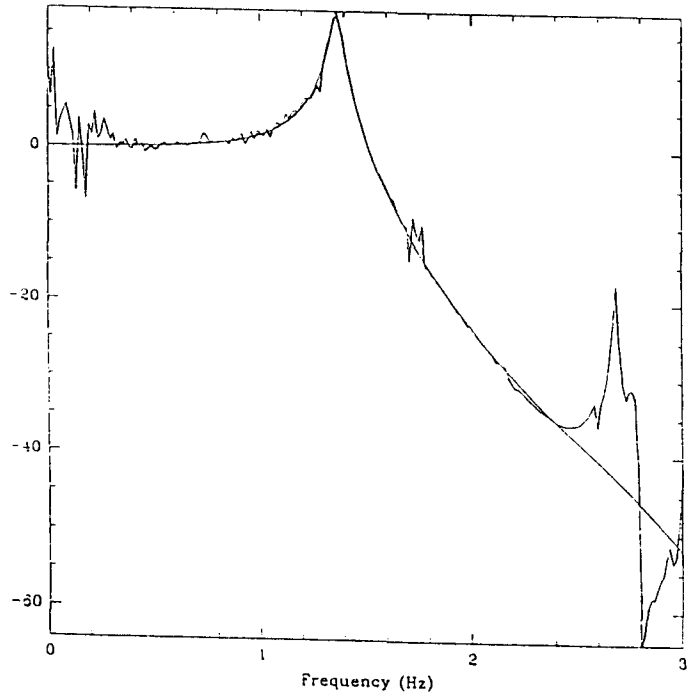

k_1=1.34e08, k_2=7.12e08, c=1.25e05
mass(kg)=6.3e0, range for fit (Hz)=5–400

Figure 7 (d)
Fit between four-pole parameter
model and experiment for
cars in shear

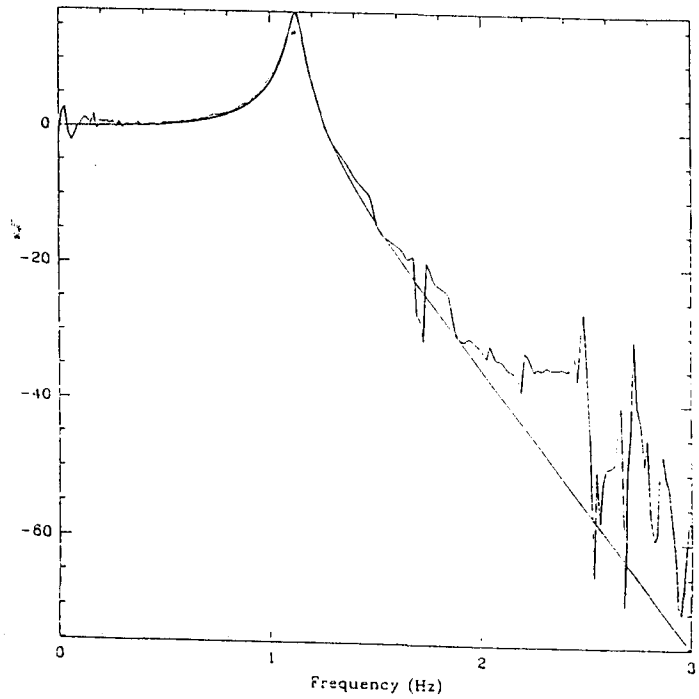

k_1=6.77e08, k_2=6.36e08, c=8.66e08
mass(kg)=5.9e0, range for fit (Hz)=5–300

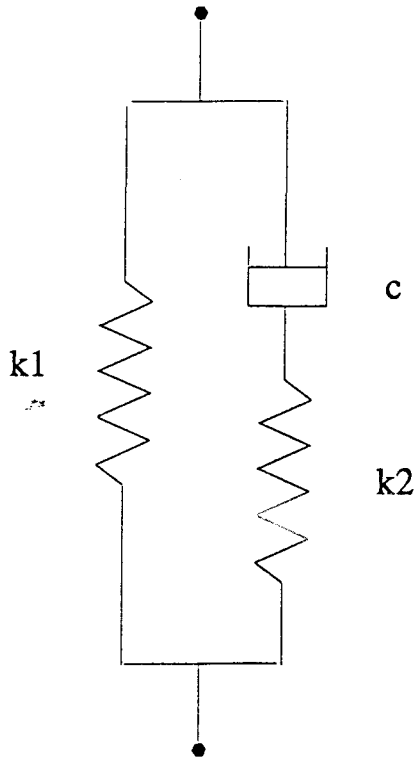

Figure 7(e). 4 Pole Spring Model

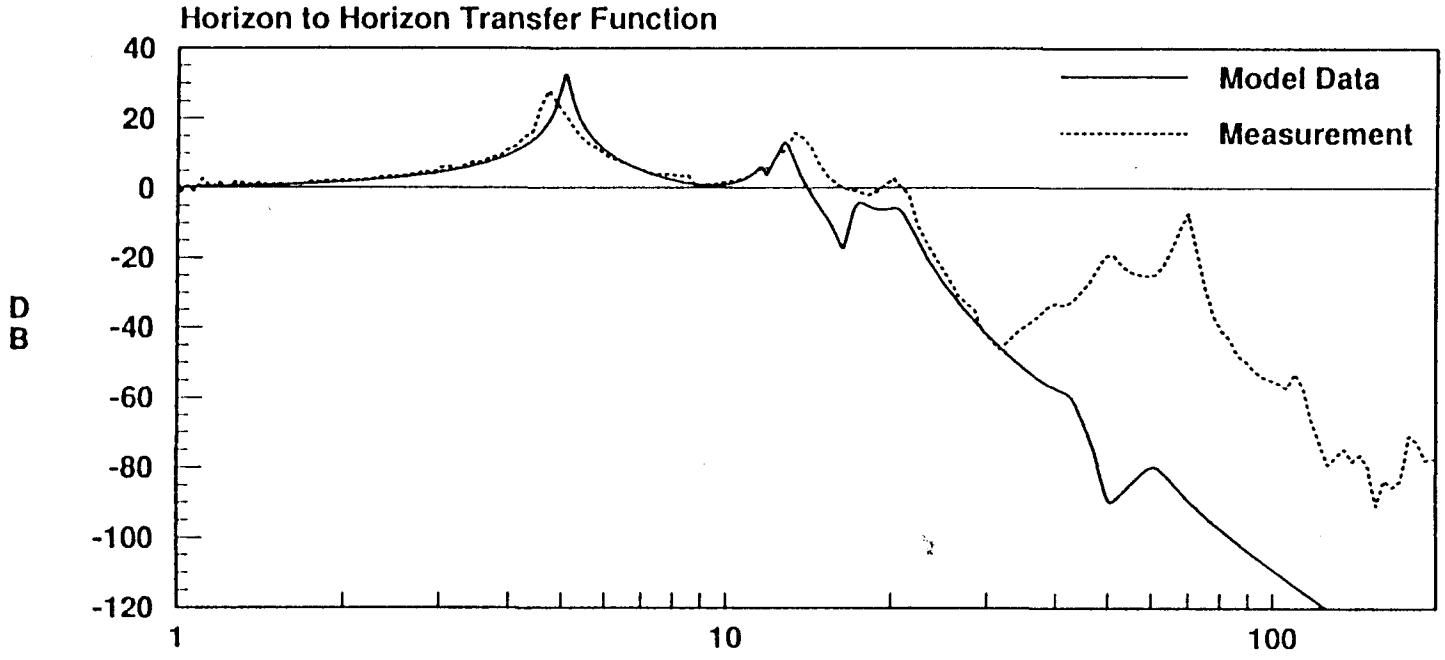

Figure 8.1

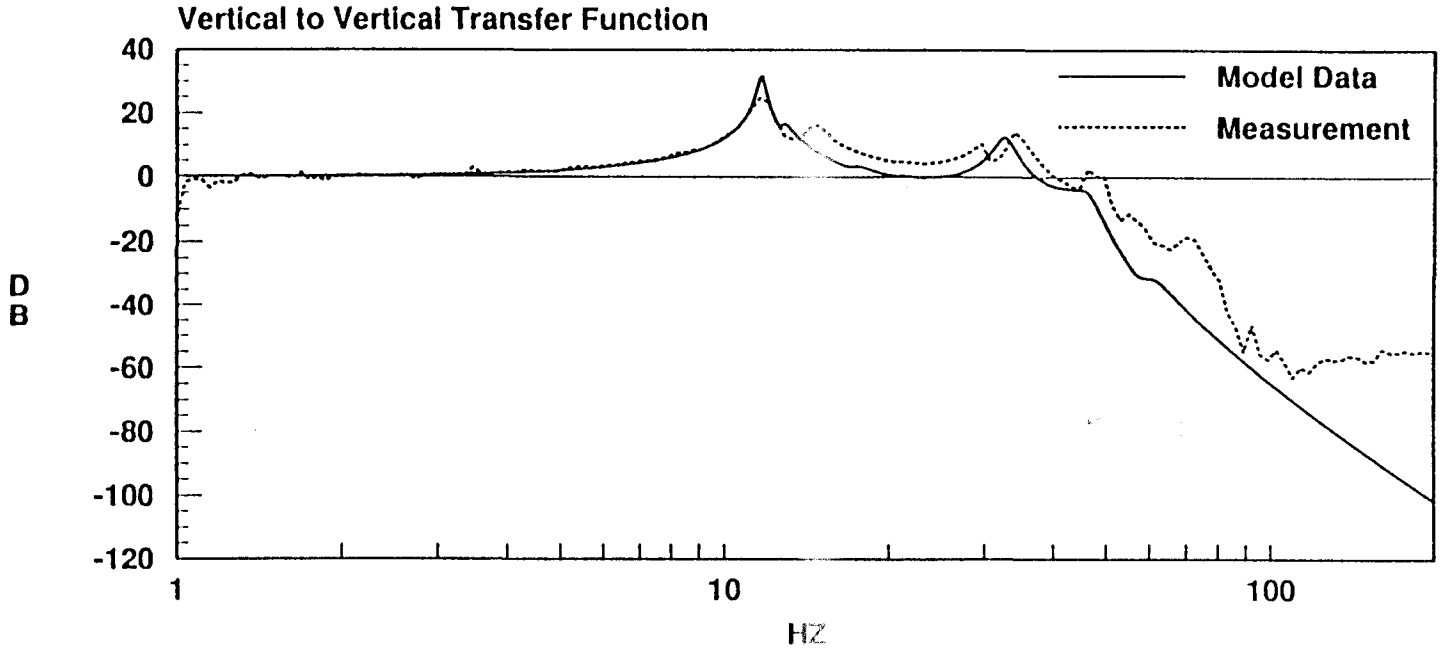

Figure 8.2

40 M Stack with Silicone Cubes and Simple Top Plate

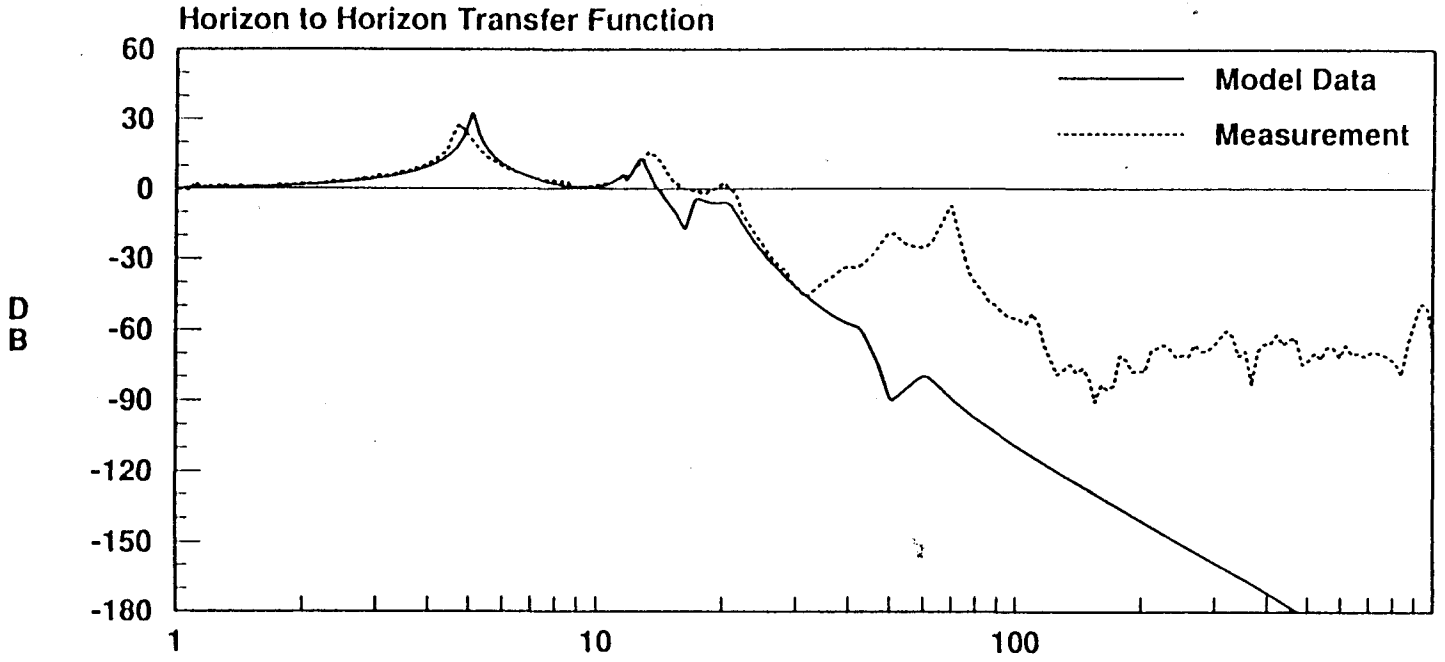

Figure 8.3

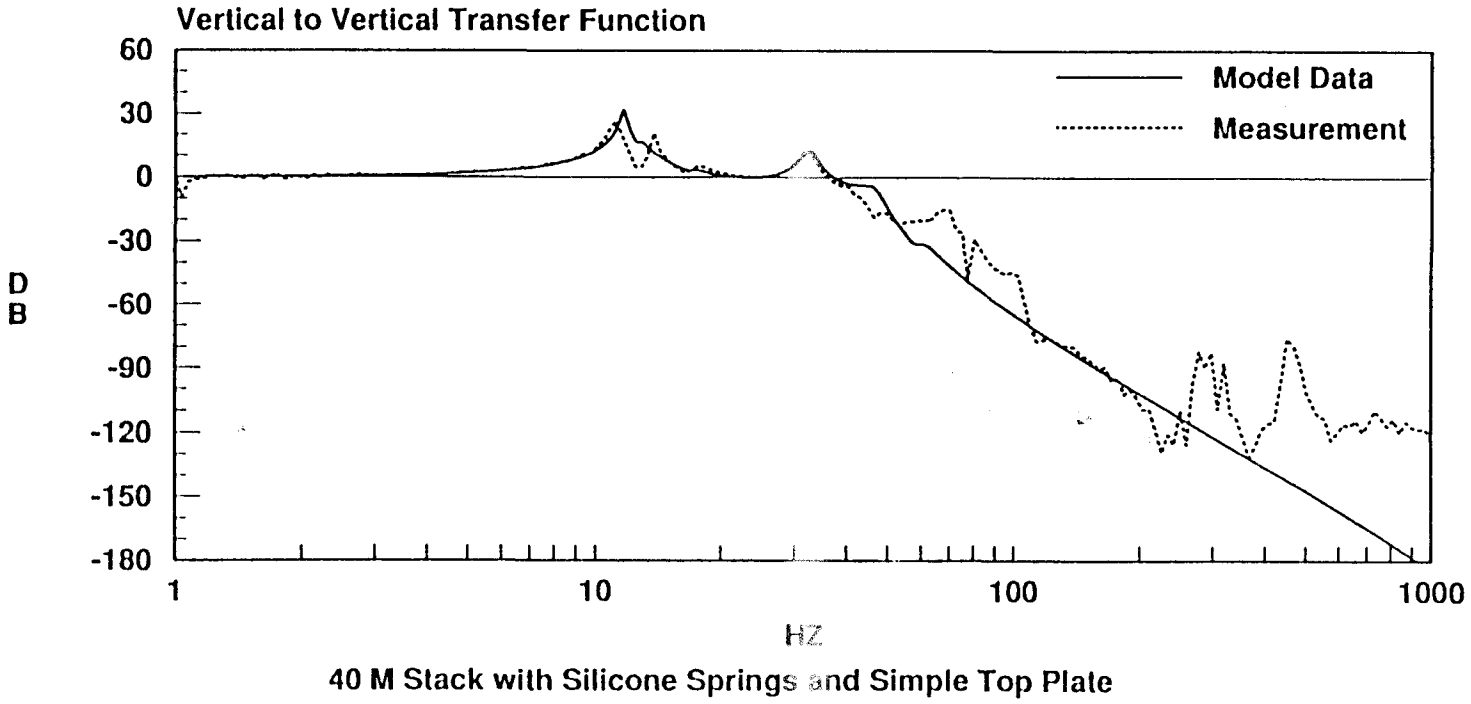

Figure 8.4

40 M Stack with Silicone Springs and Simple Top Plate

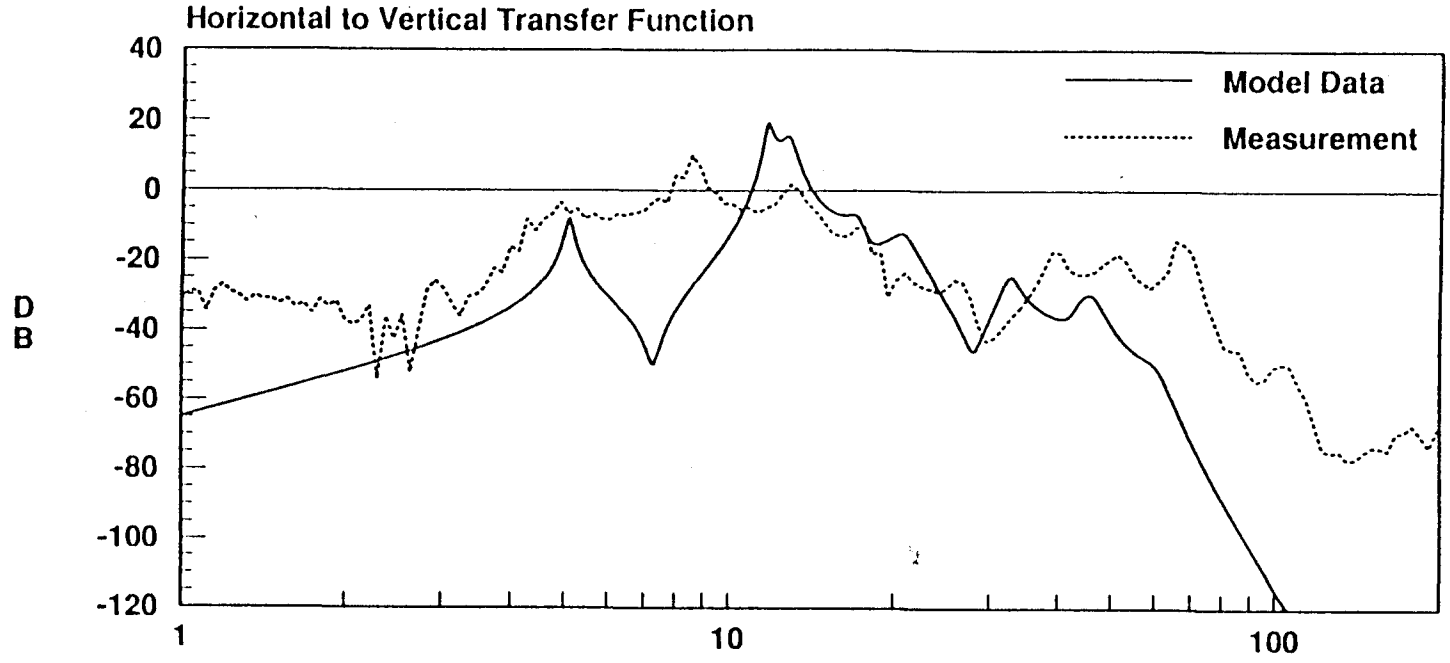

Figure 8.5

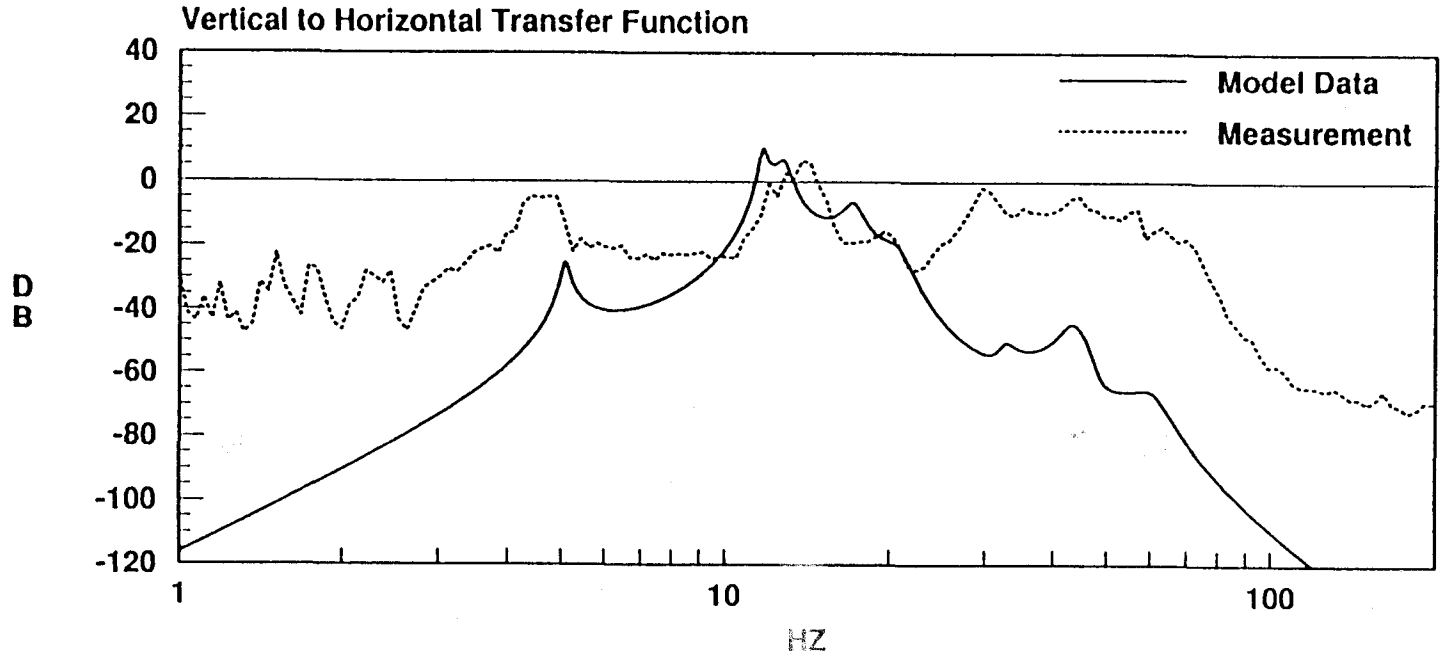

Figure 8.6

40 M Stack with Silicone Cubes and Simple Top Plate

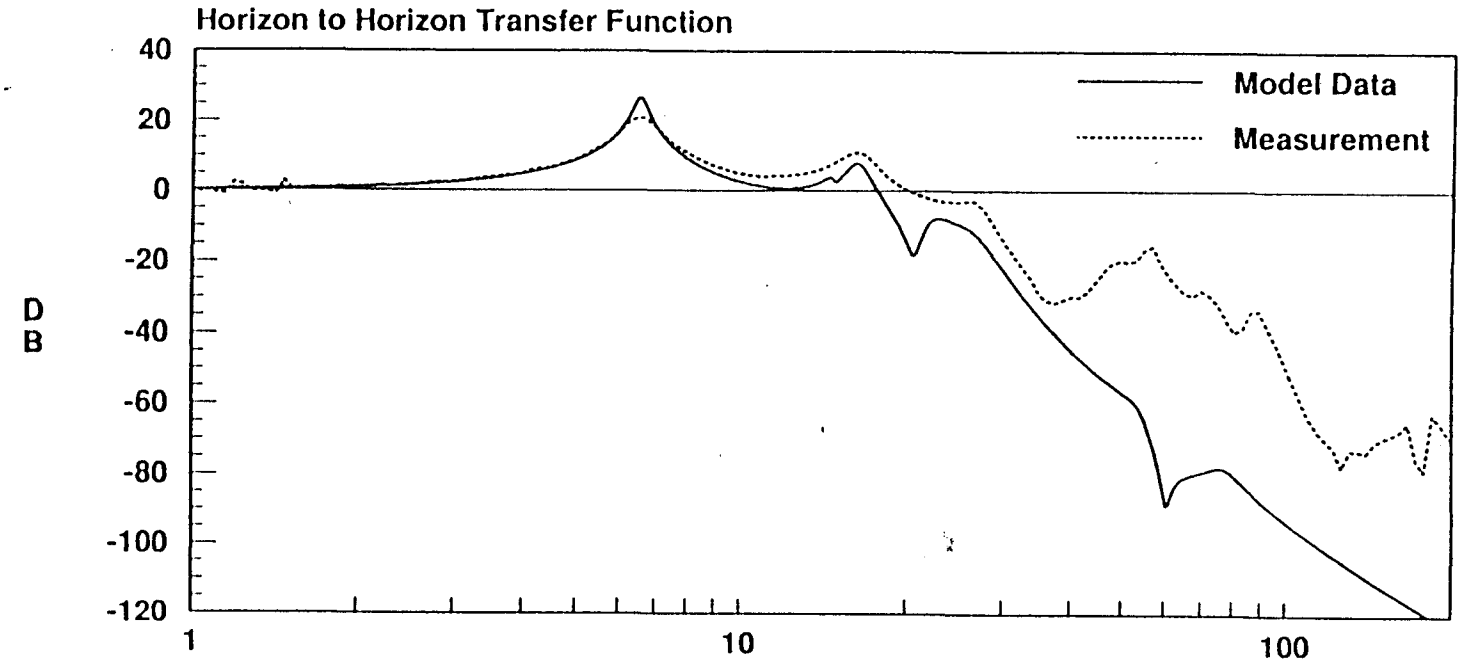

Figure 8.7

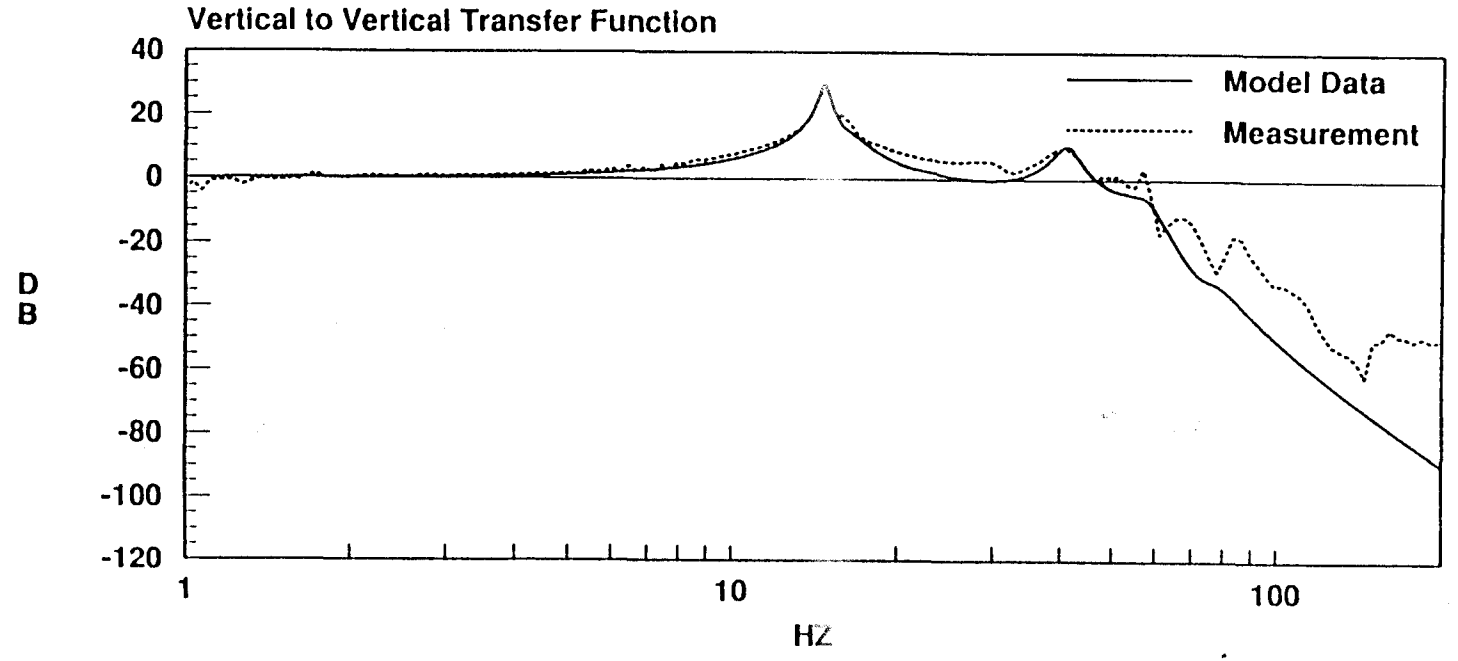

Figure 8.8

40 M Stack with Car Springs and Simple Top Plate

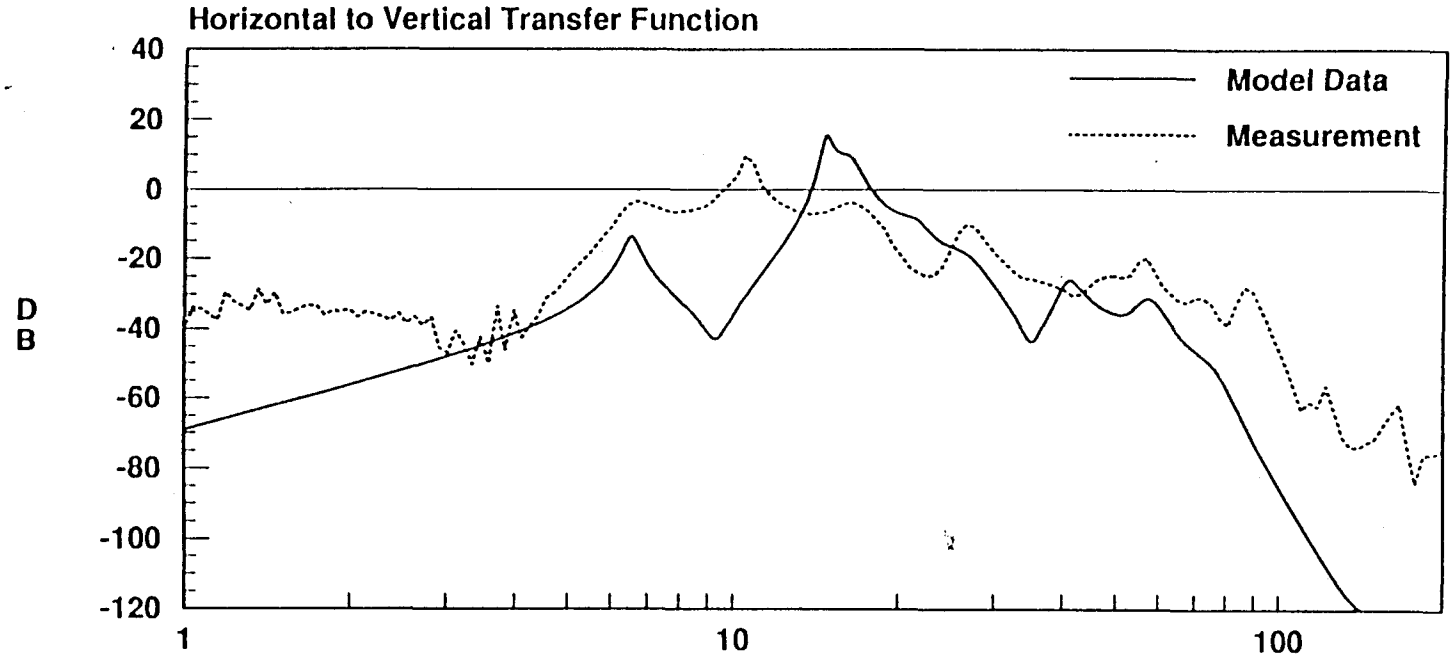

Figure 8.9

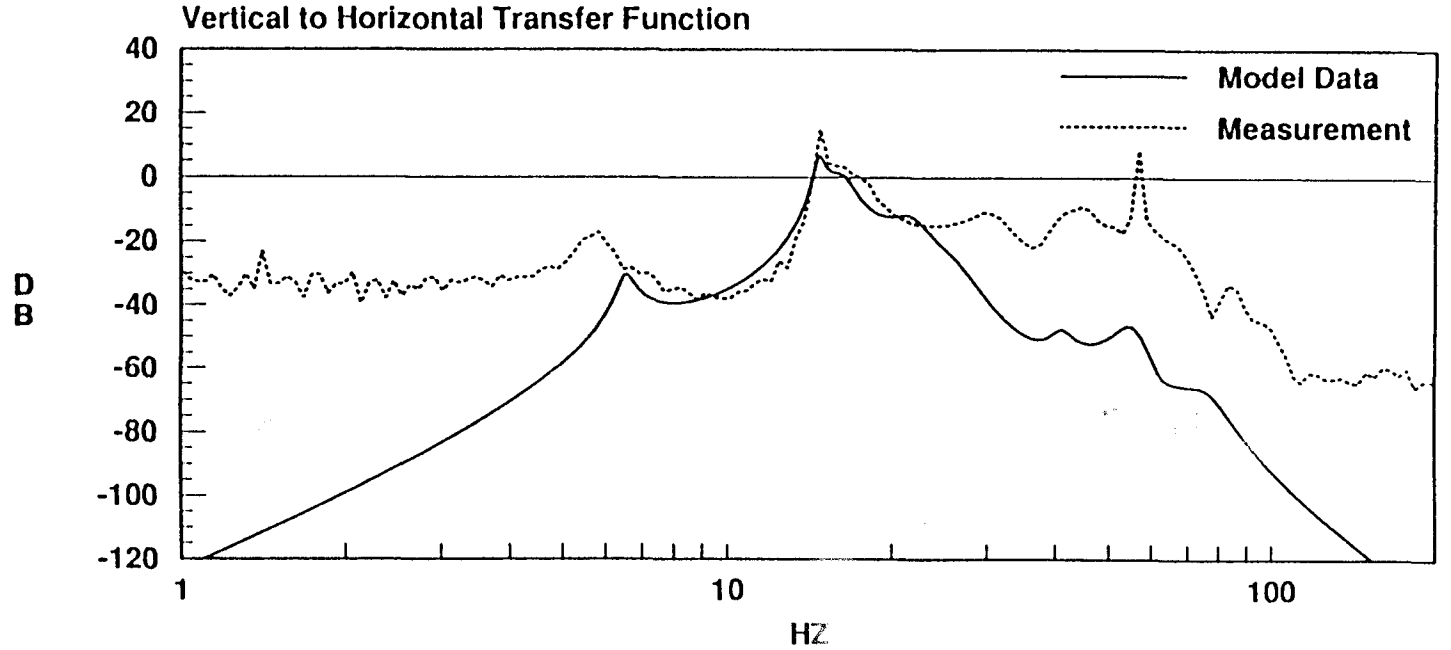

Figure 8.10

40 M Stack with Car Springs and Simple Top Plate

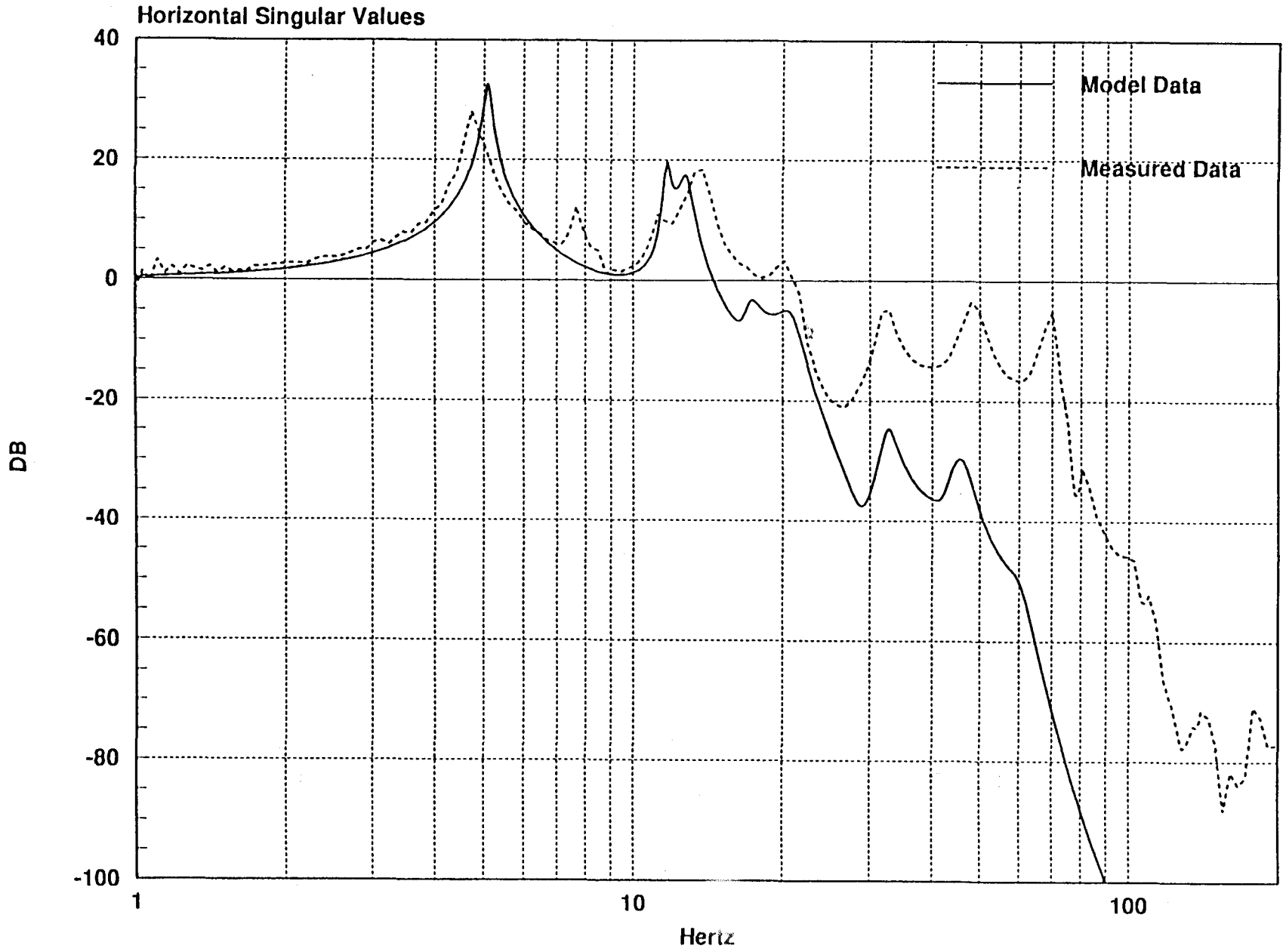

Figure 9.1 Limit on Gain of Horizontal TF for Stack with Silicone Springs

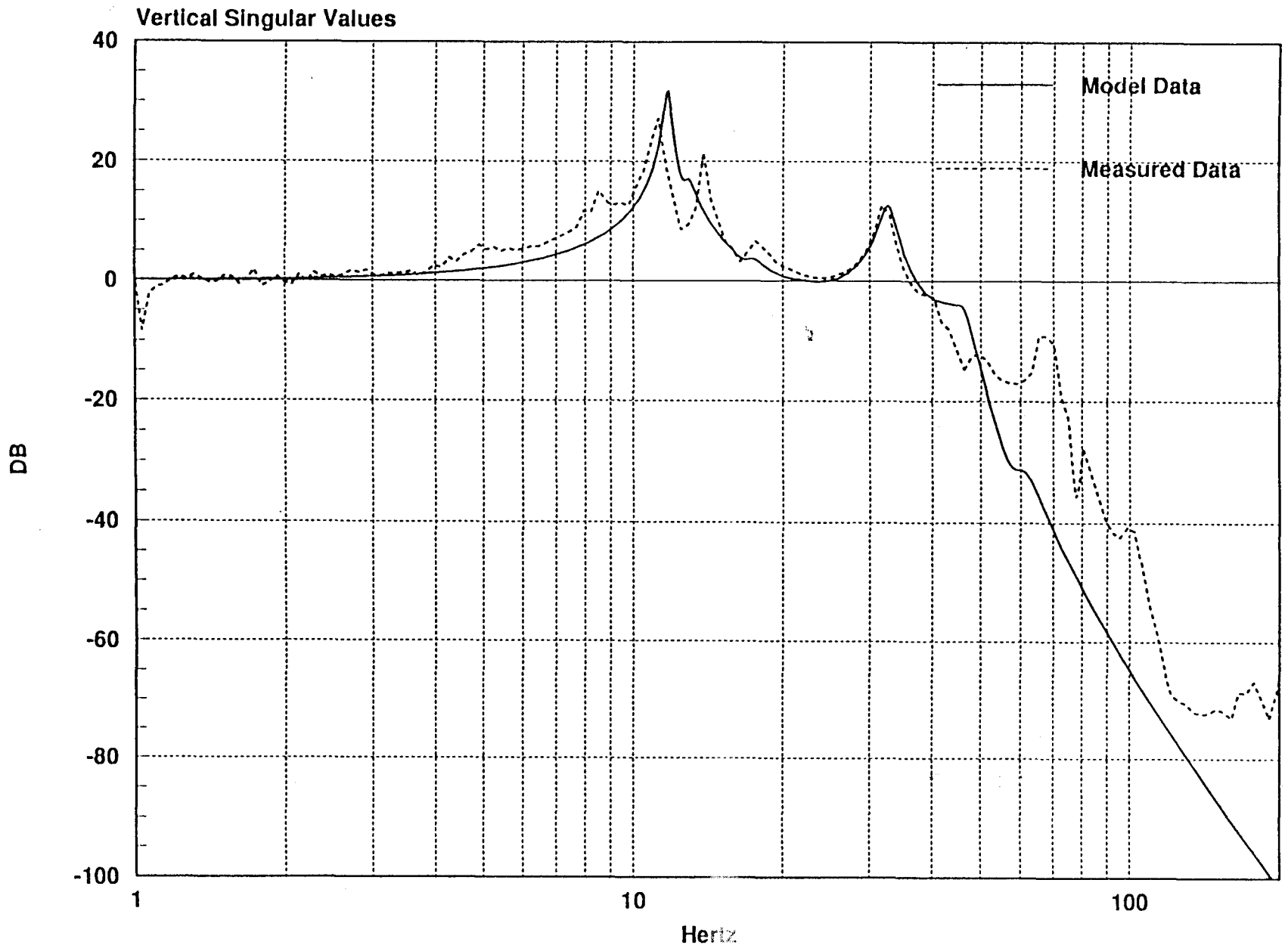

Figure 9.2 Limit on Gain of Vertical TF for Stack with Silicone Springs

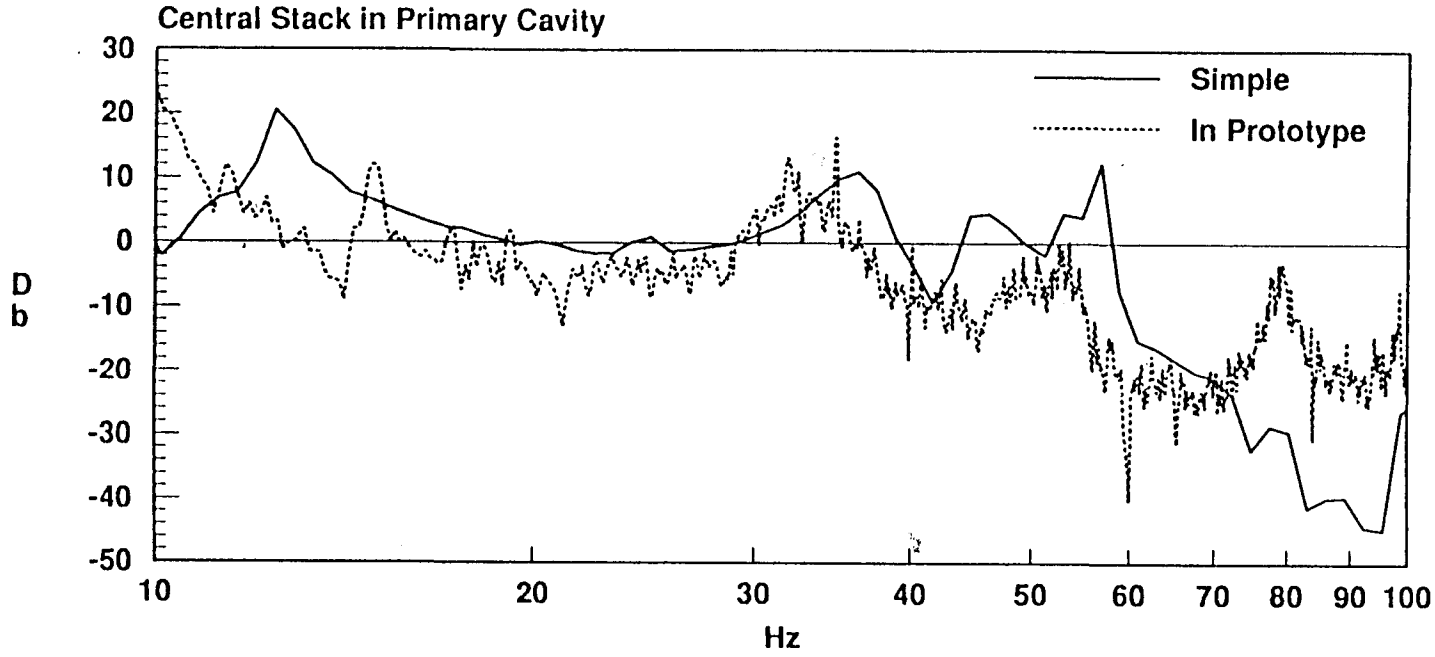

Figure 10.2

V to V TFs of Simple Stack and Stack Assembled in Prototype

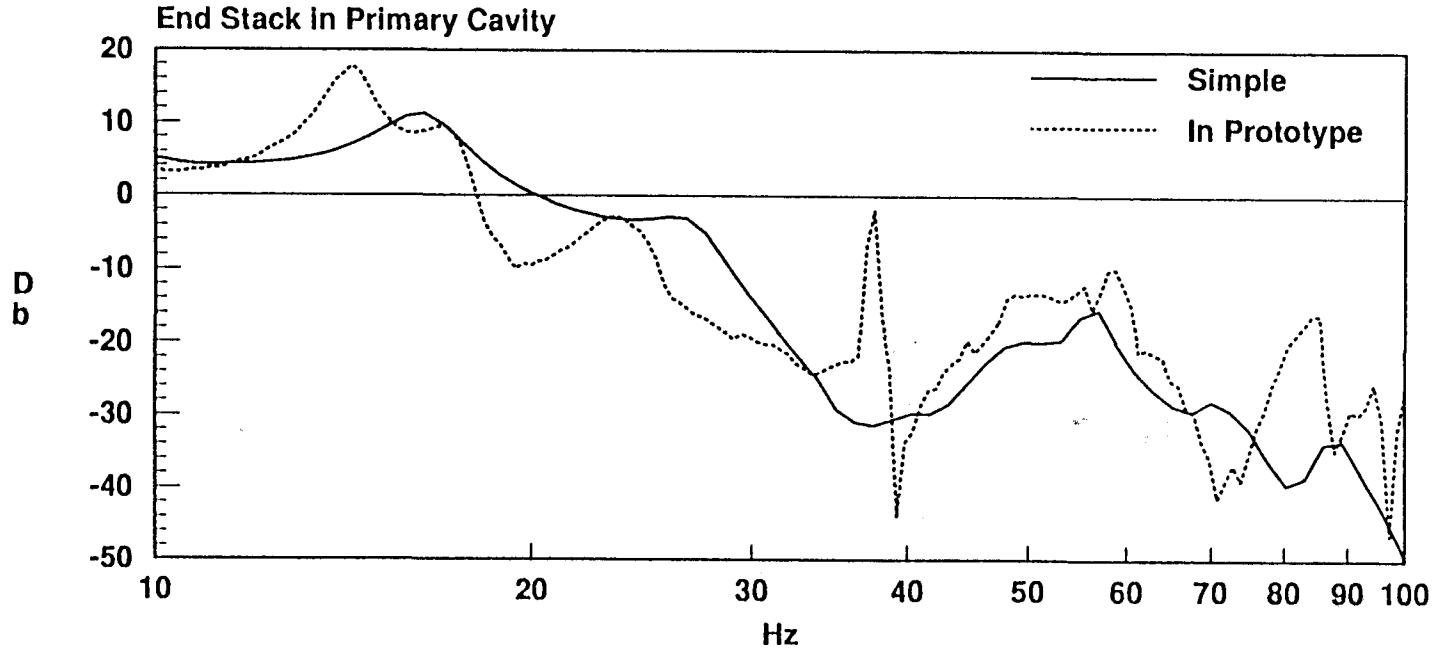

Figure 10.1

H to H TFs of Simple Stack and Stack Assembled in Prototype